Differential Coaxial Coils for Frequency Independent Deep Magnetic Focusing on Implantable Devices

Syed Ahson Ali Shah[1], Ye R Kim[1], Yun-Su Kim[1], and Chun T Rim[1]

[1]Affiliation not available

August 12, 2024

Differential Coaxial Coils for Frequency Independent Deep Magnetic Focusing on Implantable Devices

Syed Ahson Ali Shah, *Member, IEEE*, Ye R. Kim, Yun-Su Kim, *Senior Member, IEEE*, and Chun T. Rim, *Fellow Member, IEEE*

***Abstract*—Magnetic field focusing in longitudinal direction has been a missing link for three-dimensional synthesized magnetic focusing (3-D SMF). Deep magnetic focusing (DMF) by multiple coaxial coils, a sort of 3-D SMF, is firstly proposed in this paper, where magnetic field becomes maximum at the focal range in longitudinal direction. DMF is requisite for transcranial magnetic stimulation (TMS) and wireless power transfer (WPT). As the simplest DMF, a set of differential coils with opposite current direction is implemented. Optimum coil currents, coil radii, and coil distance are designed to provide with zero magnetic field at zero range and maximum magnetic field at a focal range. This DMF performance is found to be achieved with a penalty of peak magnetic field reduction. Experiments for the differential coils of diameters 10 cm and 5 cm with 3 cm gap showed 4 cm depth DMF within 6 cm diameter. Specific numbers of turns make the DMF be driven by only a single voltage source, which is firstly adopted in SMF. The frequency versatile DMF characteristic is experimentally verified for 60 Hz and 40 kHz, where 27mW is delivered to a focal point that is a demonstration for safer WPT of implantable devices.**

***Index Terms*— deep magnetic focusing (DMF), differential coils, synthesized magnetic focusing (SMF), transcranial magnetic stimulation (TMS), wireless power transfer (WPT).**

I. INTRODUCTION

MAGNETIC focusing plays a pivotal role in diverse systems, from neuro-stimulation technologies like transcranial magnetic stimulation (TMS) [1]–[2] to emerging applications like magnetic field-based wireless power transfer (WPT) [3]–[5]. It leverages magnetic fields to control and concentrate charged particle beams, enabling targeted interventions and efficient energy transfer. This is why researchers have been struggling to develop techniques and systems to control, steer, and focus the magnetic field for a variety of applications. One of successful cases is the magnetic stimulation system developed for brain activation by asymmetric current pulses to generate desired magnetic fields [1]. A microcontroller-based equipment for TMS application was proposed to activate selected brain areas; however, the system lacks the capability of magnetic field focusing [2]. Nonetheless, current TMS systems have several problems including unfocused magnetic field focusing, unintended stimulation of unwanted brain areas, and lack of precision. Similarly, in WPT applications, the growing demand of smart devices at any point in space have necessitated the development of innovative WPT systems capable of controlling and steering the magnetic field towards desired WPT receivers. Moreover, some sensitive implantable devices of a human body require precise magnetic field to specific areas for increased safety.

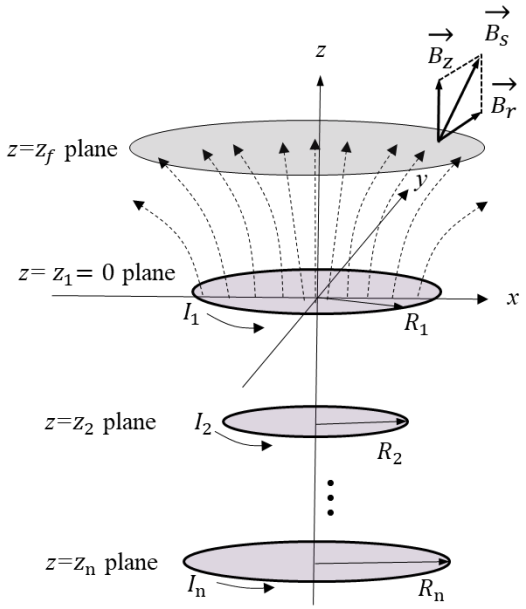

Fig. 1. General multiple coaxial coils for deep magnetic focusing (DMF).

Synthesized magnetic focusing (SMF) is an effective and systematic method for concentrating magnetic field over a restricted area of space [6]–[13]. SMF was first proposed for one-dimensional (1-D) coil arrays to focus the magnetic field in one direction, where magnetic field width was found to be a fourth of the unfocused coil [6], [7]. To steer the magnetic field in two-dimensional (2-D) axis, a 2-D SMF was also proposed for several applications including energy-efficient WPT applications [8] and high-resolution non-destructive testing (NDT) [9]. Moreover, SMF was also used for radio frequency identification (RFID) [10] as an alternative identification technology. In addition to the focused magnetic field, the SMF inevitably generates side lobes whose intensity should be much lower than the main lobe. The side lobe of SMF was effectively reduced by appropriate control of synthesized coil currents [11].

Syed Ahson Ali Shah, Yun-su Kim, and Chun T. Rim are with the Graduate School of Energy Convergence, and Ye R. Kim is with the Department of Electrical Engineering and Computer Science at Gwangju Institute of Science and Technology (GIST), Gwangju, 61005, South Korea (e-mail: sahsonas@gist.ac.kr, yunsukim@gist.ac.kr corresponding author: ctrim@gist.ac.kr, e-mail: fion1010@gm.gist.ac.kr).

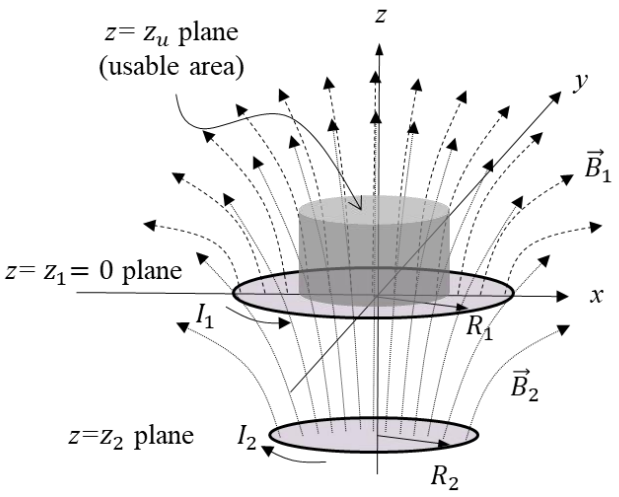

Fig. 2. Configuration of the proposed differential coils (n = 2).

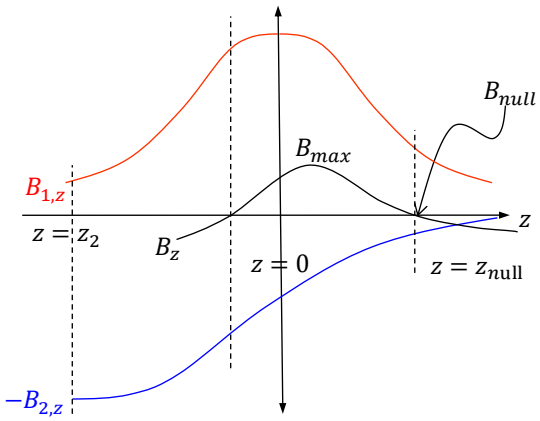

Fig. 3. Principle of differential coils at the centerline (r = 0).

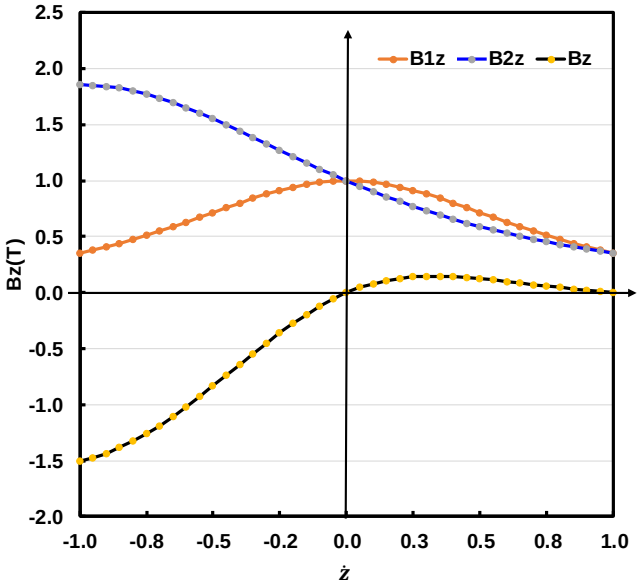

Fig. 4. Centerline magnetic flux density (r = 0) of differential coils for B_0 = 1 T, a = 1.4, b = 1.0, and c = 2.6.

It is noteworthy that the SMF theory is based on the general electromagnetic inverse problems [12]–[16], where TMS [17]–[19] are also based on. For the safety of patients, the detection of magnetic field is necessary [20],[21],[22].

For magnetic focusing applications of WPT, NDT, RFID, and TMS, high resolution of three-dimensional (3-D) SMF is mostly desirable. It is found from the 1-D SMF [6], [7] and 2-D SMF [8] that lateral direction magnetic focusing with respect to coil plane is relatively easy to get implemented; however, longitudinal direction magnetic focusing has not yet been reported, which is crucial for the 3-D SMF. Because of the nature of a coil, magnetic flux density at proximity is high and becomes low as distance increases. Deep magnetic focusing (DMF), a sort of longitudinal 3-D SMF, is highly needed in TMS and WPT, where magnetic field density is zero at proximity and becomes its peak at a focal range. Several techniques are used in the literature to generate the desired magnetic field, such as asymmetrical coils [21], magnetic field coupling model [23], biplanar coils [24], [25], and magnetic field suppression [26]. They can enhance the precision of magnetic sensors but the DMF which focuses magnetic field at a distant focal point only is quite challenging and has never been successful so far.

Note that the concept of using multiple coils to shape the magnetic field pattern has been explored in prior works. However, this study introduces a unique method for achieving precise deep-focused B-field, with control over multiple parameters such as coil currents, coil radii, distances between coils, and distances between the coils and the focusing point. This level of parameter control is critical in applications where precision and safety are key, such as in TMS and WPT.

The core contribution of this paper is the introduction of design rules that guide the procedure for developing multiple circular coil systems specifically for deep B-field focusing. This is not merely an exploration of a general concept; we aim to provide a practical framework for achieving targeted magnetic field patterns with a high degree of accuracy. The use of multiple coaxial coils with varying parameters allows for a more customized magnetic field distribution, which is not commonly seen in existing studies. In this paper, a general multiple coaxial-coil based DMF, as shown in Fig. 1, is firstly proposed and its simplest form of differential coils is implemented to demonstrate the idea. The principle of DMF is explained for the center of axis of two coils first. Then the design of coil currents, coil radii, and coil distance of the differential coils is suggested through equation-based simulation. Finally, an optimally designed DMF of differential coils is verified by FEM simulations and experiments.

II. Design of the Proposed DMF

A. Proposed Multiple Coaxial Coils for DMF

One of systematic ways of implementation of 3-D SMF is to stack 2-D coils in series with same distance. Locating coils systematically, i.e., size, configuration, spacing, and positions of coils is highly appropriate for the systematic design rule and performance [6]–[11]. So, same configuration of 2-D coils having equal spacing between each plane is desirable. For simplicity of design and isotropic magnetic field distribution

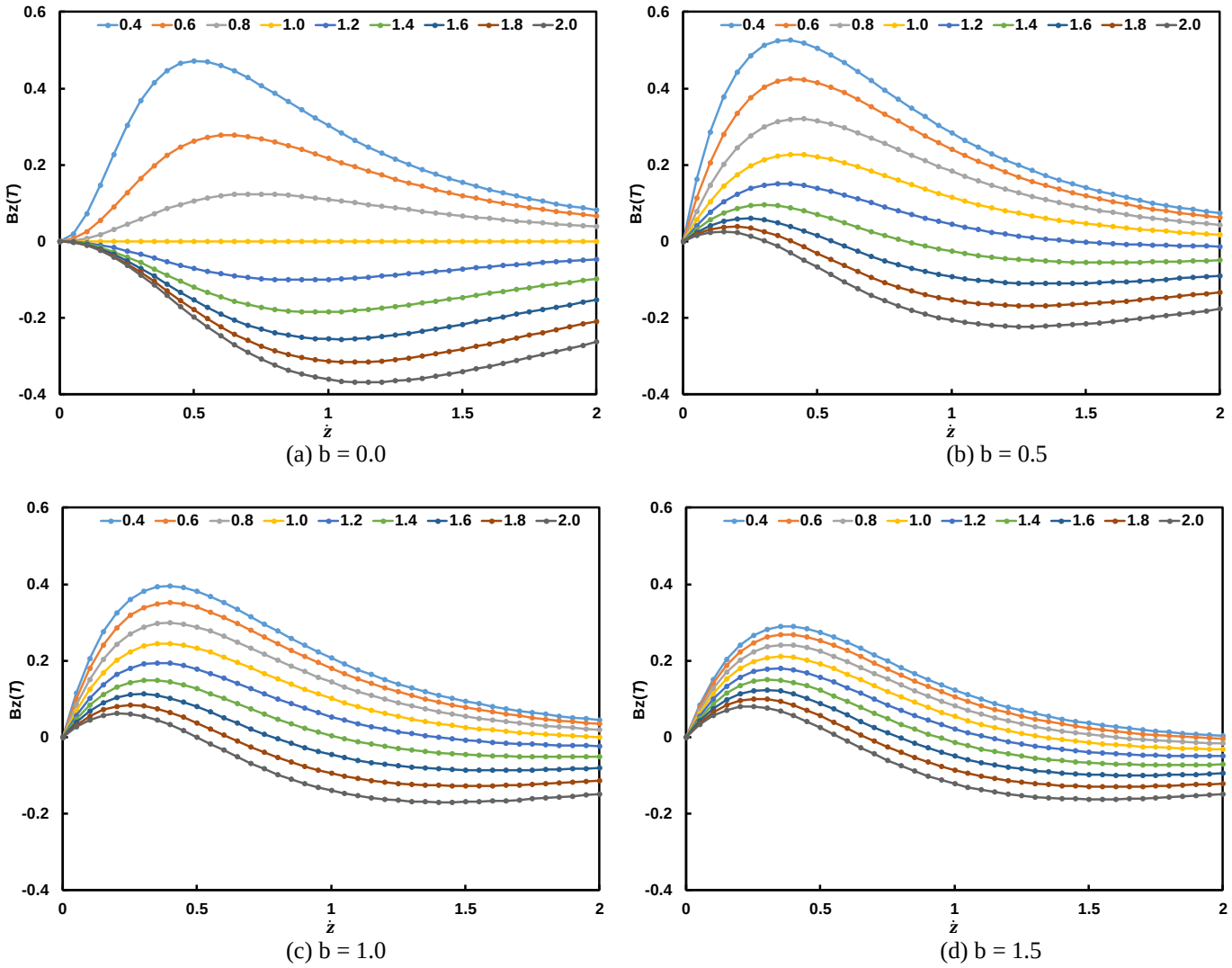

Fig. 5. Simulated centerline magnetic flux density (r = 0) of differential coils for various a and $\dot{z} \geq 0$.

with respect to z-axis, the circular type coil is chosen rather than a rectangular or other complex structures for the implementation of DMF. Fig. 1 shows the general multiple coils DMF system with coils placed in different z-planes. Variation to this 3-D SMF configuration can then be made to improve specific performances such as side lobes [11].

As shown in Fig. 1, the k-th coil current I_k $(k = 1,2,\dots,n)$, where n is the number of coils, represents the total coil currents usually composed of multi-turns. The radius of the k-th coil R_k $(k = 1,2,\dots,n)$ is arbitrary and an optimum value should be determined to provide in-depth SMF performance in the subsequent section. The magnetic flux density of the proposed DMF is the sum of each circular coil as follows:

$$\vec{B}_s \equiv \vec{B}_s(x,y,z) = \sum_{k=1}^{n} \vec{B}_k = \sum_{k=1}^{n} (B_{k,x}\vec{x} + B_{k,y}\vec{y} + B_{k,z}\vec{z})$$

$$= \sum_{k=1}^{n} (B_{k,r}\vec{r} + B_{k,z}\vec{z}) \equiv B_r\vec{r} + B_z\vec{z} = \vec{B}_s(r,z), \quad (1a)$$

$$\because\ B_{k,r}\vec{r} \equiv B_{k,x}\vec{x} + B_{k,y}\vec{y},\ k = 1,2,\dots,n,$$

$$B_r = \sum_{k=1}^{n} B_{k,r},\ B_z = \sum_{k=1}^{n} B_{k,z} \quad (1b)$$

where $\vec{x}, \vec{y}, \vec{z}$ are unit vectors of x, y, z coordinate and $B_{k,r}, B_{k,z}$ can be found from [27]-[29].

$$B_{k,r} = \frac{\mu_0 I_k \gamma}{2\pi R_k \sqrt{G}} \left[E(\rho) \frac{1+\alpha^2+\beta^2}{G-4\alpha} - F(\rho) \right],\ k = 1,2,\dots,n \quad (2a)$$

$$B_{k,z} = \frac{\mu_0 I_k}{2\pi R_k \sqrt{G}} \left[E(\rho) \frac{1-\alpha^2-\beta^2}{G-4\alpha} + F(\rho) \right],\ k = 1,2,\dots,n \quad (2b)$$

$$\because \rho = \sqrt{\frac{4\alpha}{G}},\ G = (1+\alpha)^2 + \beta^2,\ \alpha = \frac{r}{R_k},\ \beta = \frac{z}{R_k},\ \gamma = \frac{z}{r}$$

$$k = 1,2,\dots,n \quad (2c)$$

$$F(\rho) = \frac{\pi}{2} \sum_{l=0}^{\infty} \left[\frac{(2l-1)!!}{(2l)!!} \right]^2 \rho^{2l} \quad (2d)$$

$$E(\rho) = \frac{\pi}{2} \left\{ 1 - \sum_{l=1}^{\infty} \left[\frac{(2l-1)!!}{(2l)!!} \right]^2 \frac{\rho^{2l}}{2l-1} \right\} \quad (2e)$$

Note from (2b) that $\vec{r}$ vector is on x-y plane and perpendicular to z axis, as shown in Fig. 1. Because the magnetic flux density $\vec{B}_s$ is symmetrical with respect to z axis, only two vector components is needed to represent it as shown in (2a) and (2b). Equations (2d) and (2e) are the complete elliptic integral function, of the first kind and the second kind, respectively and they can be calculated for given r, z points.

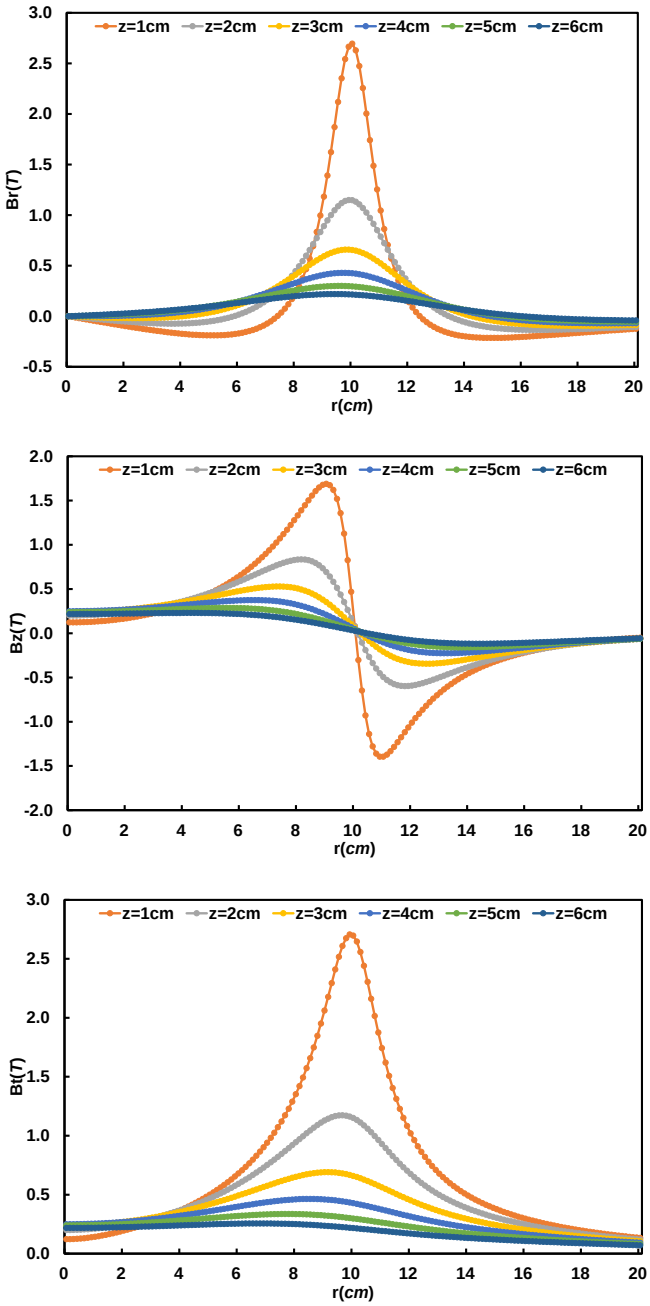

Fig. 6. Simulated offline magnetic flux distribution ($r \neq 0$) of differential coils for a = 1.0, b = 0.8, and c = 2.1.

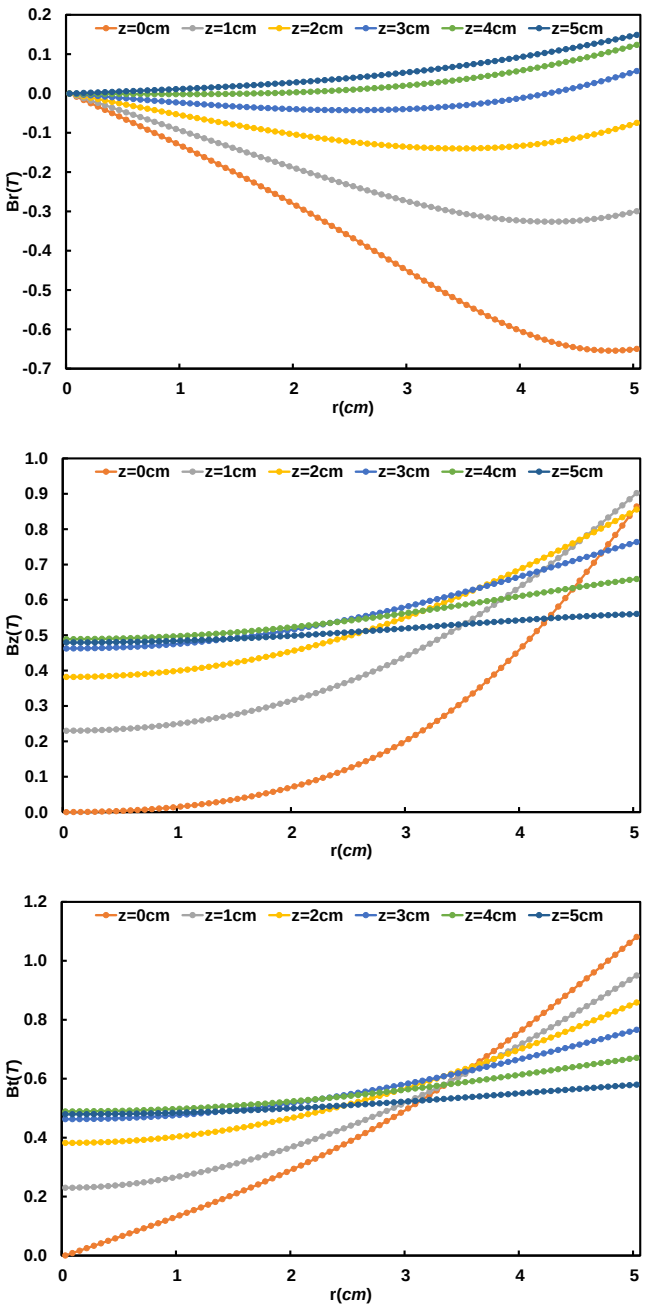

Fig. 7. Simulated offline magnetic flux distribution ($r \neq 0$) of differential coils for a = 0.5, b = 0.3, and c = 0.793.

B. Design of Differential Coils for Centerline Performance

Instead of finding a general solution of $I_k, (k = 1,2, \dots, n)$ for a general DMF, a two-coil case, i.e., n = 2 is specifically examined in this paper. As shown in Fig. 2, it is called 'differential coils' because the current direction and their associated *B*-fields of the two coils are in opposite each other. More general DMF could be designed based on the results of this research.

Unfortunately, neither physical property nor design rule is available from direct calculation of SMF equations [6]–[11]. So, to seek for underlying physics for a DMF is one of the purposes of studying this differential coil. For simplicity, the centerline behavior, i.e., *z*-axis, is examined, as shown in Fig. 3. The magnetic flux density at r = 0 is found in a very simple form from (2) as follows:

$$B_{k,r}(r = 0, z) = 0, \quad k = 1,2 \tag{3a}$$

$$B_{k,z}(r = 0, z) = \frac{\mu_0 I_k}{2R_k[1+\left(\frac{z-z_k}{R_k}\right)^2]^{1.5}}, \quad k = 1,2\,. \tag{3b}$$

Note from (3b) that the magnetic flux is a function of current, radius, and position of a coil; therefore, there is a room for manipulating the curve with these three variables. From (3b), the synthesized magnetic field of the differential coils B_z can be found as follows:

$$B_z(0,z) \equiv B_{1,z}(0,z) - B_{2,z}(0,z) = \frac{\mu_0 I_1}{2R_1[1+\left(\frac{z}{R_1}\right)^2]^{1.5}} - \frac{\mu_0 I_2}{2R_2[1+\left(\frac{z-z_2}{R_2}\right)^2]^{1.5}}. \quad (4)$$

As shown in Fig. 3, B_z may have a peak B_{max} with two null points by appropriate selection of the variables. The null points may move arbitrarily, so the wanted longitudinal magnetic field distribution could be obtained. The underlying principle is that the magnetic field of the second coil cancels out that of the first coil at distance in a different fashion of magnetic field distribution. In order to see the detail behaviors, equation (4) is normalized and further simplified as follows:

$$B_z(0,z) = \frac{\mu_0 I_1}{2R_1}\left(\frac{1}{[1+\left(\frac{z}{R_1}\right)^2]^{1.5}} - \frac{\frac{I_2}{I_1}}{R_2/R_1[1+\left(\frac{z-z_2}{R_2}\right)^2]^{1.5}}\right) \equiv B_0\left(\frac{1}{[1+\dot{z}^2]^{1.5}} - \frac{c}{a[1+\left(\frac{\dot{z}+b}{a}\right)^2]^{1.5}}\right) = B_z(0,\dot{z}). \quad (5a)$$

$$\because B_0 \equiv \frac{\mu_0 I_1}{2R_1},\ a \equiv \frac{R_2}{R_1},\ b \equiv -\frac{z_2}{R_1},\ c \equiv \frac{I_2}{I_1},\ \dot{z} \equiv \frac{z}{R_1} \quad (5b)$$

For in-depth magnetic focusing, it is appropriate to make a null point of B_z be near z = 0. It is deemed to use the DMF $z \geq 0$ only. Under this condition, a design condition is derived from (5a) as follows:

$$B_z(0,\dot{z}_{null}) = B_0\left(\frac{1}{[1+\dot{z}_{null}^2]^{1.5}} - \frac{c}{a[1+\left(\frac{\dot{z}_{null}+b}{a}\right)^2]^{1.5}}\right) = 0 \quad (6a)$$

$$\therefore\ c = \frac{a[1+\left(\frac{\dot{z}_{null}+b}{a}\right)^2]^{1.5}}{[1+\dot{z}_{null}^2]^{1.5}} = a[1+\left(\frac{b}{a}\right)^2]^{1.5} \text{for } \dot{z}_{null} = 0 \quad (6b)$$

By appropriate selection of coil current c for any given a and b, the null point $\dot{z}_{null}$ always exists as identified from (6b). Especially, $\dot{z}_{null}$ = 0 is one of preferences because it makes B_{max} point as close as possible so that B_{max} can be maximized. Negative $\dot{z}_{null}$ is not prohibited in theory; however, inside the coil is deemed to be unused in this paper.

Fig. 4 is a simulation result for the normalized case of B_0= 1 T with a = 1.4, b = 1.0, c = 2.6 example, which has two null points at $\dot{z}$ = 0 and $\dot{z} \cong$ 1.0. Note the normalized $B_{max} \cong$ 0.2 T, which is much less than the original magnetic flux density of the first coil of 1.0 T. This reduced magnitude of magnetic flux density of the DMF is the result of subtraction to get the longitudinal magnetic focusing.

To maximize B_{max} with small z_{null} is the design goal of the proposed differential coils; therefore, normalized B_z of (5) with B_0= 1 T is plotted for various a and b under (6) condition, as shown in Fig. 5.

For b = 0.0, a large B_{max} is achieved, however, there is no z_{null}. The negative values of B_z for a > 1 is not a problem for practical applications though.

For b = 0.5, z_{null} exists and a trade-off between B_{max} and z_{null} is possible. For example, B_{max}= 0.15 T at $\dot{z}$ = 0.35 and $\dot{z}_{null}$= 1.45 for a = 1.2 and c = 1.53.

For b = 1.0, z_{null} exists for many a's and a trade-off between B_{max} and z_{null} is possible. For example, B_{max}= 0.25 T at $\dot{z}$ = 0.40 and $\dot{z}_{null}$= 2.0 for a = 1.0 and c = 2.83.

For b = 1.5, z_{null} exists for many a's and a trade-off between B_{max} and z_{null} is also possible. For example, B_{max}= 0.27 T at $\dot{z}$ = 0.35 and $\dot{z}_{null}$= 1.9 for a = 0.6 and c = 11.71. For this case, the second coil current is very large, so this solution might not be a good choice.

From the above discussions, it is found that $0.3 \leq b \leq 1.0$ would be an appropriate range and that B_{max} exists around $\dot{z}$ = 0.40. Note that to finalize the design of the proposed differential coils is too early because the above discussions so far is about for the centerline behavior only. The performance of other areas should be explored, which is given in the subsequent section.

C. Design of Differential Coils for Offline Performances

As shown in Fig. 1, the proposed differential coils have $\vec{B}_s(r, z)$ of r component as well as z component of (1) and (2). Bearing the conceptual design results of previous section in mind, let's look at the offline ($r \neq 0$) performances as well. The synthesized magnetic flux distribution of the differential coils is the vector sum of two coils, i.e., $\vec{B}_s$=$\vec{B}_1$+$\vec{B}_2$. In order to get zero magnetic flux at $z = z_{null}$, not only B_z but also B_r must be zero, which is never easy to get. The selection of parameters a, b, and c under (6) is tried for different z plane, as shown in Fig. 6. For this simulation, it is assumed that R_1= 10.0 cm and B_0= 1 T.

Large non-zero values are observed around r = 10 cm and in-depth magnetic focusing of (6) is restricted to $r \leq 3$ cm for this example. So, the usable area, as defined in Fig. 2, is $0 \leq z_u \leq z_{null}$, $r \leq 3$ cm. The magnitude of synthesized magnetic field density is found from (1) as follows:

$$B_t \equiv |\vec{B}_s| = |\sum_{k=1}^{n}(B_{k,r}\vec{r} + B_{k,z}\vec{z})| = |B_r\vec{r} + B_z\vec{z}| = \sqrt{B_r^2 + B_z^2}. \quad (7)$$

Focusing attention to the usable area, extensive search for optimum parameters of a, b, and c under (6) is made and one of optimum cases is shown in Fig. 7.

Comparing $B_t(r = 3, z = 0)$ = 0.499 with $B_t(r = 0, z = 4)$= 0.489, the maximum usable area of the example of Fig. 7 is found to be $0 \leq z_u \leq z_{null}$, $r < 3$ cm. B_{max} is achieved at the focal length $z = z_f$. Note that B_t for $z = 0$ should be at its minimum and less than the maximum B_t of the usable area for in-depth magnetic focusing applications.

III. FEM-Based Maxwell Simulations

A. Simulation Setup

In order to validate the proposed DMF calculations, FEM-based simulations are performed in Ansys Maxwell for a = 0.5, b = 0.3, and c = 0.79, where $R_1 = 10$ cm and $R_2 = 5$ cm. The procedure included modeling of the DMF coils, setting up the simulation parameters, and analyzing the results in the Magnetostatic solver. For the DMF coils, copper wire was used. Each coil of the DMF system was excited through the current source. Fine meshing was assigned to each coil for accurate

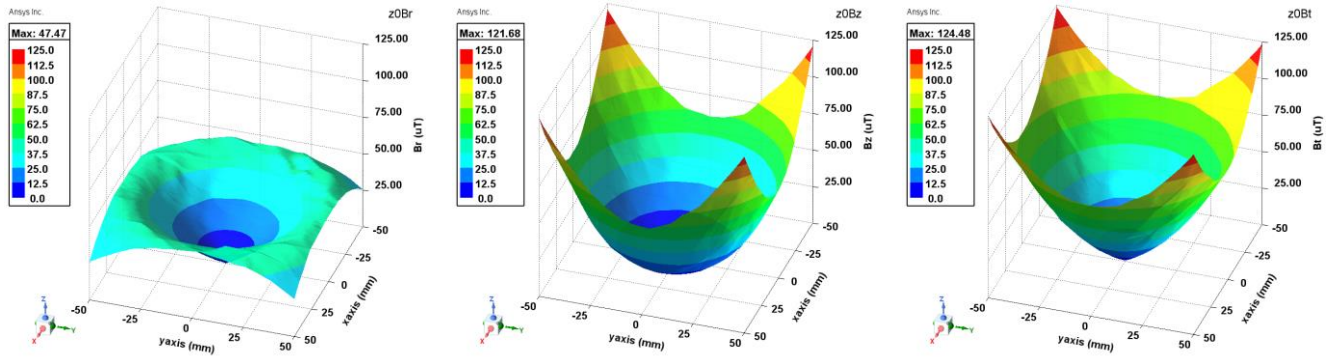

(a) $z = 0\ cm$

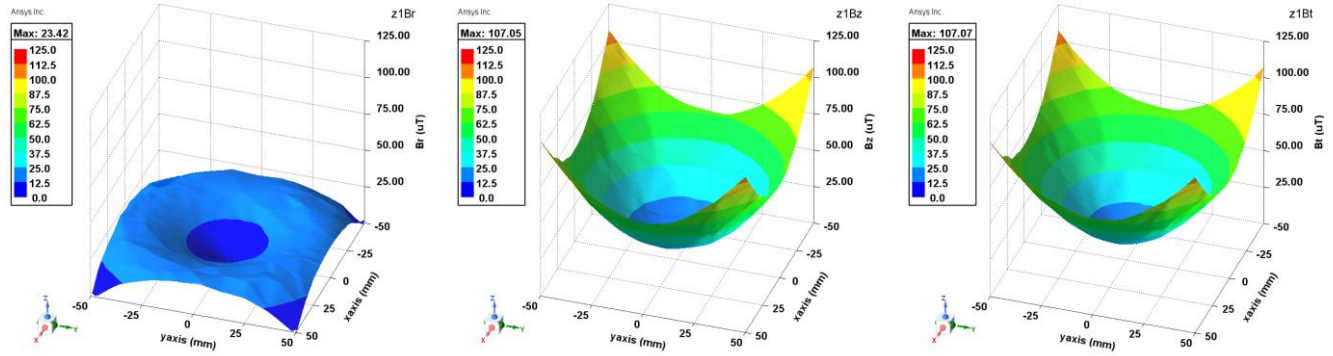

(b) $z = 1\ cm$

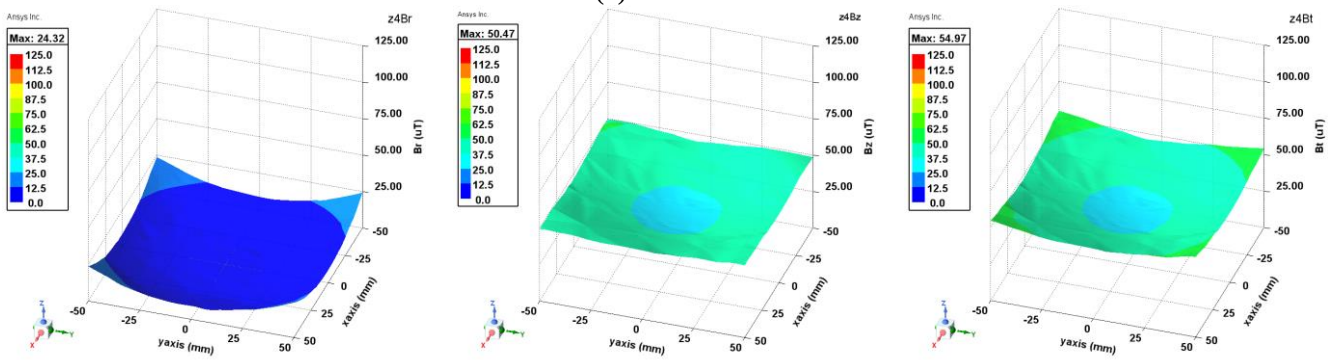

(c) $z = 4\ cm$

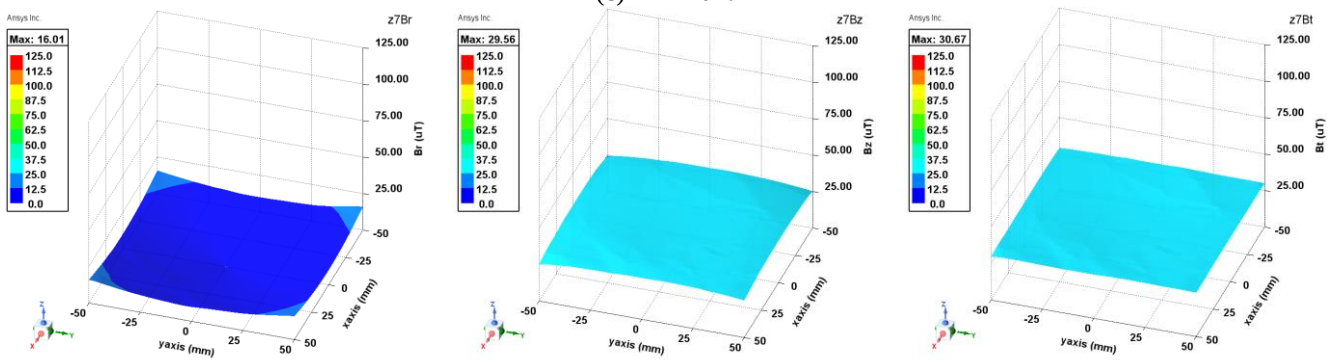

(d) $z = 7\ cm$

Fig. 8. Simulated $\vec{B}_s$ for a = 0.5, b = 0.3, and c = 0.79 to verify basic performance of deep magnetic focusing.

representation of physical system in simulation domain. The DMF coils and receiver planes were encapsulated by a vacuum box to represent open boundary conditions.

B. Simulation Results

As shown in Fig. 8, the simulated 3D-surface plots of the magnetic field for various z planes are well matched with the calculations and experiments of Fig. 10. It can be clearly

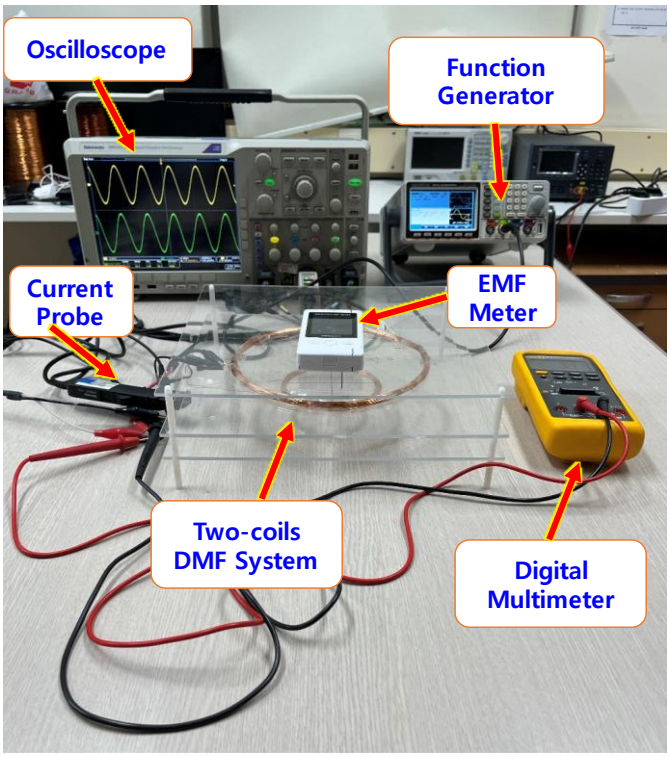

Fig. 9. Experiment kit for a = 0.5, b = 0.3, and c = 0.79 to verify basic performance of deep magnetic focusing at 60 *Hz*.

visualized that the useable area is within $r \leq 3\ cm$. It is worthy to note that it is not possible to obtain exactly zero B field, but near-zero can be achieved. Due to the circular symmetry of the coils, the magnetic field is symmetric throughout the x-y plane.

IV. Experimental Verifications

A. *Experiments for Basic DMF at 60 Hz*

As shown in Fig. 9, an experimental kit was fabricated for the proposed DMF of a = 0.5, b = 0.3, and c = 0.79, where $R_1 = 10\ cm$ and $R_2 = 5\ cm$. The two coils are connected in series; therefore, a single voltage source can actuate the system instead of two independent sources, which is the case of conventional SMF. The numbers of turns for each coil are set to $N_1 = 100$ and $N_2 = 79$ to cope with the theoretically calculated currents. For experimental verification, $I_1 = 11.4\ mA$ and $I_2 = 9.0\ mA$ is used. Note that ± 0.2 % quantized error due to the integer number of turns is inevitable for the experiment kit because c = 0.790 for experiment has been slightly changed from the theoretical value 0.793. The resistance and inductance of the coils are measured as 9.5 Ω and 5.1 *mH*, respectively. The self-resonant frequency of the two-coils DMF system due to parasitic capacitance is experimentally measured as 136 *kHz*, where the parasitic capacitance is found to be 269 *pF*.

For precise experimental verification of the proposed DMF system, the measurement frequency is selected as 60 *Hz* because the SMF performance should be ideally independent of frequency. A function generator MFG-2260MRA was used as the voltage source and an EMF meter, TENMARS was used for the measurement of magnetic field, as shown in Fig. 9.

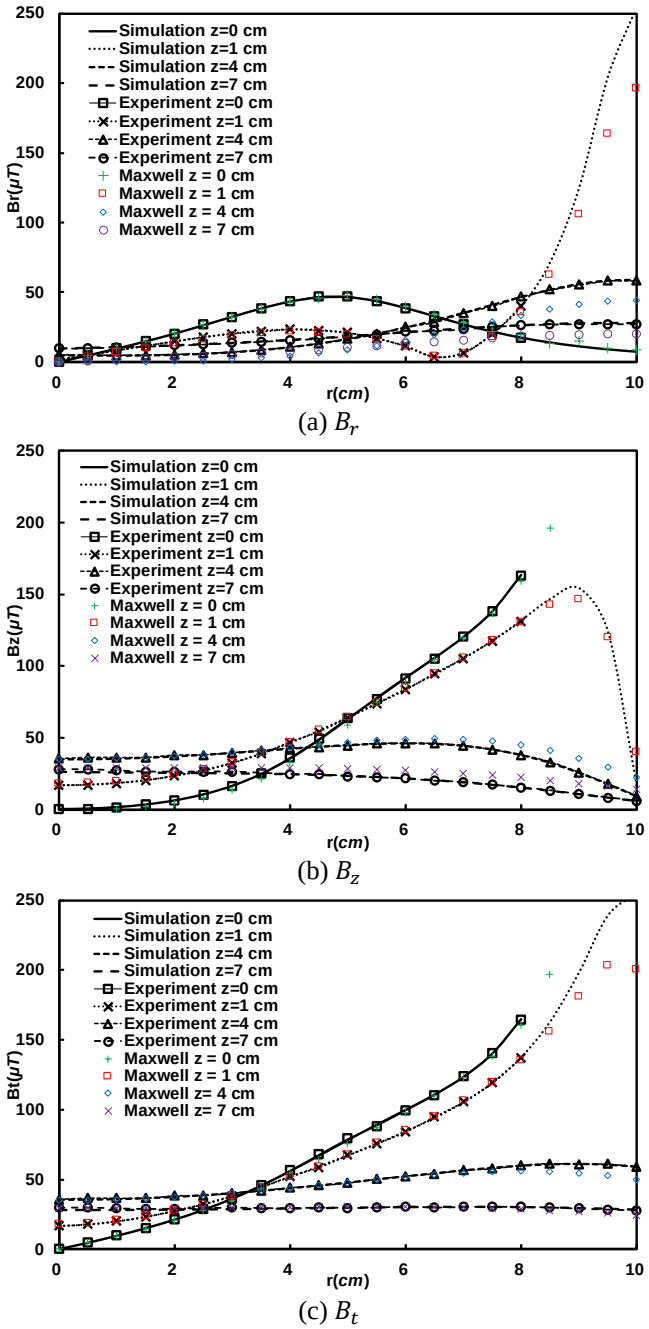

(a) B_r

(b) B_z

(c) B_t

Fig. 10. Calculated, simulated, and measured $\vec{B}_s(r, z)$ a = 0.5, b = 0.3, and c = 0.79 at 60 *Hz*.

As shown in Fig. 10, the measured magnetic field shows high agreement with simulation. Proximity of coils was not measured. As noted from Figs. 10 (b) and (c), the measured magnetic field B_z and B_t increase as z increases up to 4 *cm*, which is the peak within the range of $r < 3\ cm$. As shown in Fig. 10 (a), the measured B_r becomes large especially $r > 4\ cm$, which is why the useable area becomes $(z, r) \leq (4\ cm, 3\ cm)$. Note that the experimental data points for $r > 8\ cm$ could not been measured due to the width of the Tesla meter, which could effectively measure up to 8 cm for $z = 0\ cm$ and $z = 1\ cm$. Nonetheless, the performance of the DMF system is consistent in most cases. Considering the size of the main coil of $R_1 = 10\ cm$ in the proposed design, the useable area of the proposed

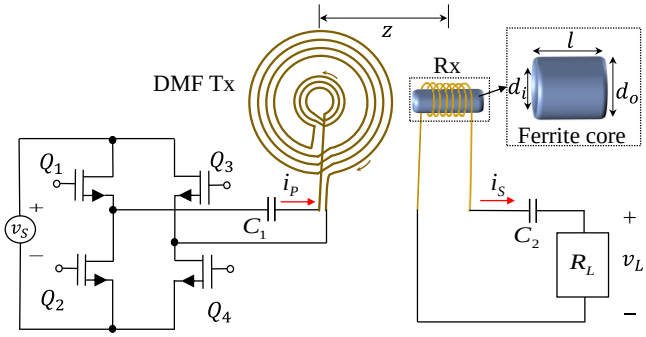

Fig. 11. The overall circuit configuration of the proposed DMF for the WPT experiment at 40 *kHz*. $C_1 = 2.84\ nF, C_2 = 694\ nF, l = 15.5\ mm, d_o = 12.1\ mm,\ d_i = 7.3\ mm.$

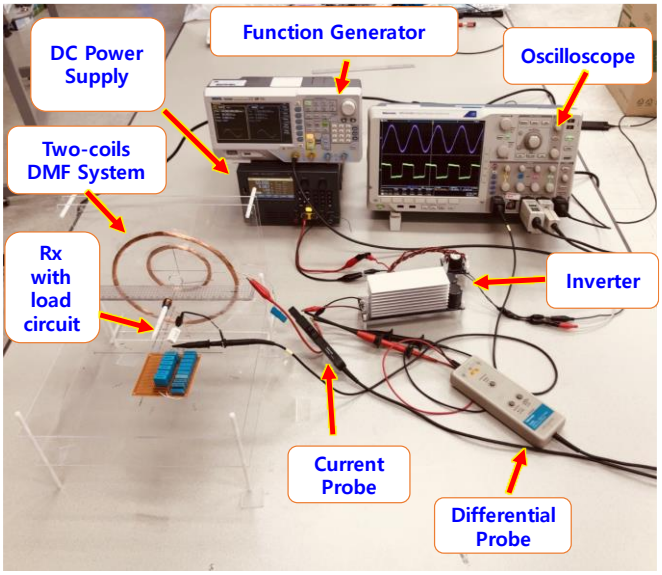

Fig. 12. Experiment kit for a = 0.5, b = 0.3, and c = 0.79 to verify DMF-based WPT system at 40 *kHz*.

differential coil-based DMF becomes of 40 % of R_1 in longitudinal direction and 30 % of R_1in radial direction.

B. Experiments for WPT of DMF at 40 kHz

To show the efficacy of the proposed DMF system for WPT applications on small receivers (Rx) of implantable devices, the experimental kit was modified to include a small Rx at some distance from the DMF transmitting coil (Tx) and an inverter. Fig 11 shows the configuration of the proposed DMF-based WPT system, operating at 40 *kHz*, which is sufficiently lower than the aforementioned parasitic resonance frequency of 136 *kHz*. The DMF Tx is connected with a series capacitor C_1 of 2.84 nF, which is used to tune the DMF Tx to operate at the resonant frequency of 40 *kHz*. Note that all other design specifications of the DMF system for this experiment were kept the same as those described in the previous section. The Rx is composed of a coil with 20 turns wound around a cylindrical ferrite core. A series resonant capacitor C_2 of 694 nF is used with the Rx inductance L_x of 22.8 μH for maximum power delivery to the load R_L. The total currents of coils are $I_1 = 41.2\ A$ and $I_2 = 32.6\ A$, respectively. Fig. 12 shows the measurement setup to demonstrate the WPT operation at 40 kHz.

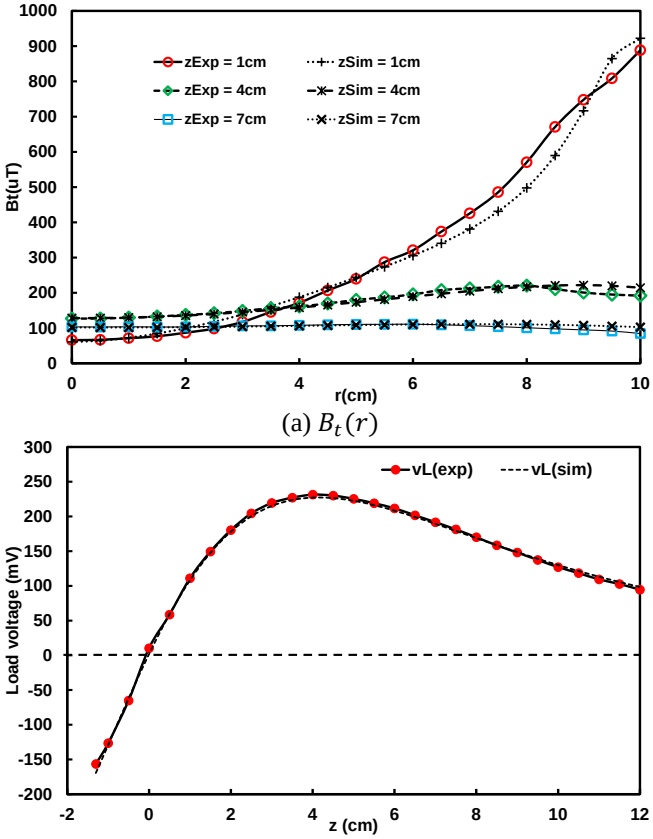

(a) $B_t(r)$

(b) $V_L(z)$

Fig. 13. Measured B_t from the load voltage (V_L) along (a) radial axis for different z and (b) measured V_L for central axis with respect to z at 40 *kHz*.

The induced voltage at the Rx for R_L of 30.0 Ω is measured for different radial positions at $z = 1\ cm$, $z = 4\ cm$, and $z = 7\ cm$, and the experimental *B*-field is determined, as shown in Fig. 13(a). Due to the parasitic capacitance of the DMF coil, switching harmonics at the parallel resonance frequency was observed in the received voltage signal. So, FFT was taken for the measured voltage v_L and the fundamental component only was recorded. The simulated and measured B_t's at 40 *kHz* for $z = 1\ cm$, $z = 4\ cm$, and $z = 7\ cm$ are in fairly good agreement with each other. The presence of slight differences may be attributed to the erroneous rotation of the Rx coil to capture the rotating *B*-field. Overall, the experimental results of Fig. 13(a) for 40 *kHz* shows high correlation with the measured B_t of Fig. 10(c) for 60 *Hz*, which ensures the most important feature of the DMF that the focusing behavior is independent of the operating frequency.

Moreover, the induced voltage at the central axis with respect to z were also measured to demonstrate the focusing behavior of the proposed DMF system, as shown in Fig. 13(b). The measured V_L increases as z increases at first, which is contrary to conventional WPT systems that is typically decreasing. Then it becomes maximum at $z_f = 4\ cm$, where the receiving power P_L reaches to 27 mW and V_L is 231mV for a load R_L= 2.0 Ω.

Further increase in *z* results in the load voltage drop gradually. Therefore, this characteristic of DMF should be beneficial for the WPT of implantable devices where magnetic field is safely mitigated for other areas than the focused point.

V. Conclusions

A new longitudinal magnetic focusing technique of DMF has been demonstrated. An optimum differential coil set as the simplest example of the proposed DMF is designed. It is found that the DMF gets longitudinal focusing capability with a penalty of reduced peak magnetic field. Longitudinally 4 *cm* in-depth DMF within 6 *cm* diameter is achieved for the differential coils of diameters of 10 *cm* and 5 *cm* with separation distance of 3 *cm*. The frequency independent DMF operation is verified by experiments for both 60 *Hz* and 40 *kHz*, which shows the possibility of safer WPT applications for implant devices.

By appropriate selection of turn-ratios of each coil and connection of coils in series, the proposed DMF could be driven by only a voltage source instead of multiple voltage sources of conventional SMF cases. This is an innovation in SMF drivers and can be used in general for other SMF drivers. Minimizing quantization errors due to integer number of turns of each coil is an open design issue for future SMF drivers.

More generalized DMF with multiple coaxial coils of $n > 2$ may have better longitudinal magnetic focusing characteristics with less sidelobe, which is left for future work. Moreover, TMS-based technical aspects are to be analyzed and validated in the future study.

Acknowledgment

This work was supported by NRF Grants NN39130 and RS-2024-00427153 funded by the Korea government (MSIT). The authors thank to Mr. W. J. Kang for his support.

References

[1] E. Basham, Z. Yang and W. Liu, "Circuit and Coil Design for In-Vitro Magnetic Neural Stimulation Systems," *IEEE Trans. on Biomedical Circuits and Systems*, vol. 3, no. 5, pp. 321-331, Oct. 2009.

[2] A. M. Pernía et al., "Equipment for Repetitive Transcranial Magnetic Stimulation," *IEEE Trans. on Biomedical Circuits and Systems*, vol. 14, no. 3, pp. 525-534, June 2020.

[3] Y. Jia et al., "A mm-Sized Free-Floating Wirelessly Powered Implantable Optical Stimulation Device," *IEEE Trans. on Biomedical Circuits and Systems*, vol. 13, no. 4, pp. 608-618, Aug. 2019.

[4] J. Kim, S. Park, S. Oh, Y. Huh, J. Cho and J. Oh, "Cage-Embedded Crown-Type Dual Coil Wireless Power Transfer Based Microwave Brain Stimulation System for Untethered and Moving Mice," *IEEE Trans. on Biomedical Circuits and Systems*, vol. 17, no. 2, pp. 362-374, April 2023.

[5] S. Pahlavan and S. J. Ashtiani, "Rotation-Tolerant Wireless Power Transmission Scheme with Smart Positioning for Cognitive Research on Moving Animals," *IEEE Trans. on Biomedical Circuits and Systems*, vol. 18, no. 1, pp. 123-130, Feb. 2024.

[6] J. P. Cheon, B. H. Choi, J. H. Kim, and Chun T. Rim, "Introduction to Synthesized Magnetic Field Focusing Technology," *APMC 2014*, Nov. 2014, pp. 1019-1021.

[7] Bo H. Choi, Ji H. Kim, Jun P. Cheon, and Chun T. Rim, "Synthesized Magnetic Field Focusing Technology using a current-controlled coil array," *IEEE Trans. Magnetics Letter*, vol. 7, Jan. 2016.

[8] Ji H. Kim, Bo H. Choi, Hoi R. Kim, and Chun T. Rim, "2-D Synthesized Magnetic Field Focusing Technology with Loop Coils Distributed in a Rectangular Formation," *IEEE Trans. on Industrial Electronics*, vol. 66, no. 7, pp. 5558-5566, July 2019.

[9] C. Liu et al., "Synthesized Magnetic Field Focusing for the Non-Destructive Testing of Oil and Gas Well Casing Pipes Using Pulsed Eddy-Current Array," in *IEEE Transactions on Magnetics*, vol. 58, no. 9, pp. 1-10, Sept. 2022, Art no. 6201710, doi: 10.1109/TMAG.2022.3186548.

[10] Min W. Kim, Bo H. Choi, Ji H. Kim, Yeon J. Cho, Min S. Kim, Guy R. Lee, Jeong H. Kim, Gyu H. Cho, Chun T. Rim, "High Resolution Synthesized Magnetic Field Focusing for RF Barcode Applications," *IEEE Trans. on Industrial Electronics*, vol. 65, no. 1, pp. 597-607, Jan. 2018.

[11] Ji H. Kim, Bo H. Choi, Hoi R. Kim, Chun T. Rim, and Yun-Su Kim, "Single-variable-input Active Sidelobe Suppression Method for Synthesized Magnetic Field Focusing Technology and its Optimization," *IEEE Trans. on Industrial Electronics*, vol. 67, no. 11, pp. 9813-9823, Nov. 2020.

[12] Sabatier, P. C. "On Geophysical Inverse Problems and Constraints." *Journal of Geophysics* 43.1 (1977): 115-137.

[13] Parker, Robert L. "Understanding Inverse Theory." *Annual Review of Earth and Planetary Sciences* 5.1 (1977): 35-64.

[14] Sarvas, Jukka. "Basic Mathematical and Electromagnetic Concepts of the Biomagnetic Inverse Problem." *Physics in Medicine & Biology* 32.1 (1987): 11.

[15] Parker, Robert L. *Geophysical inverse theory*, Vol. 1. Princeton university press, 1994.

[16] Egbert, Gary D., and Anna Kelbert. "Computational Recipes for Electromagnetic Inverse Problems." *Geophysical Journal International* 189.1 (2012): 251-267.

[17] Cohen, David, and B. Neil Cuffin. "Developing a More Focal Magnetic Stimulator. Part I: Some Basic Principles." *Journal of Clinical Neurophysiology* 8.1 (1991): 102-111.

[18] J. Ruohonen, R.J. Ilmoniemi, "Focusing and Targeting of Magnetic Brain Stimulation using Multiple Coils," *Med. Biol. Eng. Comput.* 36, 297–301 (1998).

[19] Im, C-H., and Chany Lee. "Computer-aided Performance Evaluation of a Multichannel Transcranial Magnetic Stimulation System." *IEEE Transactions on Magnetics* 42.12 (2006): 3803-3808.

[20] J. Liu, C. Nie and H. Xiong, "Multichannel Synchronous Real-Time Transcranial Magnetic Stimulation Magnetic Field Detection System Based on FPGA," *IEEE Transactions on Instrumentation and Measurement*, vol. 71, pp. 1-13, 2022, Art no. 4009313, doi: 10.1109/TIM.2022.3212528.

[21] B. Han et al., "Asymmetric Cylindrical Coils Design for Uniform Magnetic Field," *IEEE Transactions on Instrumentation and Measurement*, vol. 72, pp. 1-10, 2023, Art no. 6009710, doi: 10.1109/TIM.2023.3311064.

[22] Ching-Yao Chan, "Magnetic sensing as a position reference system for ground vehicle control," *IEEE Transactions on Instrumentation and Measurement*, vol. 51, no. 1, pp. 43-52, Feb. 2002, doi: 10.1109/19.989896.

[23] H. Pang et al., "Design of Highly Uniform Field Coils Based on the Magnetic Field Coupling Model and Improved PSO Algorithm in Atomic Sensors," *IEEE Transactions on Instrumentation and Measurement*, vol. 71, pp. 1-11, 2022, Art no. 1502611, doi: 10.1109/TIM.2022.3201500.

[24] J. Yang, X. Zhang, B. Han, J. Wang and L. Wang, "Design of Biplanar Coils for Degrading Residual Field in Magnetic Shielding Room," *IEEE Transactions on Instrumentation and Measurement*, vol. 70, pp. 1-10, 2021, Art no. 6010110, doi: 10.1109/TIM.2021.3108493.

[25] Z. Ding, Z. Huang, M. Pang and B. Han, "Design of Bi-Planar Coil for Acquiring Near-Zero Magnetic Environment," *IEEE Transactions on Instrumentation and Measurement*, vol. 71, pp. 1-10, 2022, Art no. 6001310, doi: 10.1109/TIM.2022.3151939.

[26] Q. Shao et al., "Comprehensive Structural Parameter Optimal Design of Electric Heaters With Magnetic Field Suppression for Atomic Sensors," *IEEE Transactions on Instrumentation and Measurement*, vol. 72, pp. 1-10, 2023, Art no. 9004910, doi: 10.1109/TIM.2023.3314810.

[27] Simpson, James C., et al. "Simple Analytic Expressions for the Magnetic Field of a Circular Current Loop," *No. NASA/TM-2013-217919*, 2001.

[28] R. A. Schill, "General Relation for the Vector Magnetic Field of a Circular Current Loop: a Closer Look," *IEEE Transactions on Magnetics*, vol. 39, no. 2, pp. 961-967, March 2003.

[29] W. R. Symthe, *Static and Dynamic Electricity*, vol. 290, 2nd ed., New York, NY, USA: McGraw-Hill, 1968, pp. 270-271.

Syed Ahson Ali Shah (Ph.D) received the B.Sc. degree in Telecommunication Engineering from the University of Engineering and Technology, Pakistan, in 2015 and Ph.D. in Electronic Engineering, Hanyang University, Korea, in 2022. He has been a Postdoc. with Hanyang University for 2022-2023 and with GIST now. To date, he has published several journal and conference papers. He is interested in wireless communications, wireless power transfer, and synthesized magnetic field focusing.

Dr. Ahson has received IETE MN SAHA Memorial Award and Gold Medal for best Application-Oriented Paper, in 2018. He has also received Bronze Paper Award at IEEE Student Paper Contest, Seoul, in 2019, in 2021, and in 2022. He has also won 3rd Best Student Paper Award in 2021 Competition arranged by the Korean Institute of Electromagnetic Engineering and Science (KIEES). His PhD Thesis has been recognized as one of the excellent dissertations and received the Best PhD Thesis Award in overall university and the only in Electronic Engineering Department.

Ye R. Kim is pursuing the B.S. degree in Electrical Engineering and Computer Science from the Gwangju Institute of Science and Technology (GIST), South Korea.

Her research interests include wireless power transfer systems, magnetific field focusing, and power electronics.

Yun-Su Kim (S'14–M'16–SM'21) received the B.S. and Ph.D. degrees in electrical engineering from Seoul National University, Seoul, Korea, in 2010 and 2016, respectively. He worked for Korea Electrotechnology Research Institute (KERI) as a Senior Researcher from 2015 to 2017.

He joined the Faculty of the Gwangju Institute of Science and Technology (GIST) in 2018, where he is currently an Associate Professor in the Graduate School of Energy Convergence. He is an Associate Editor of IEEE Transactions on Sustainable Energy since 2023. He was a Director of the Korean Society for New and Renewable Energy and the Korean Institute of Electrical Engineers. His research interests include distribution network, distributed energy resources, microgrid, artificial intelligence, and wireless power transfer.

Chun T. Rim (Ph.D, FIEEE) received the B.S. degree with Honor in EE from the Kumoh Institute of Technology (KIT), Korea, in 1985, and the M.S. and Ph.D. degrees in EE from the Korea Advanced Institute of Science and Technology (KAIST), Korea, in 1987 and 1990, respectively. For 2007-2016, he was an associate professor at KAIST. Since 2016, he became a full professor at the Gwangju Institute of Science and Technology (GIST), Korea. For 2018-2021, he was the President of Korean Energy Technology Evaluation and Planning (KETEP). Since 2021, he was the President of Korean Energy Economics Institute (KEEI). He has authored or coauthored 200 technical papers, written 19 books, and holds 160 patents (awarded and pending). He is the author of the books, Phasor Power Electronics, Springer, 2016, and Wireless Power Transfer for Electric Vehicles and Mobile Devices, Wiley, 2017. He won numerous awards, including the Best Paper Award of IEEE TPEL in 2015 and J-ESTPE in 2016 both in wireless power transfer (WPT). He became the IEEE Fellow in 2020 and now he is a Co-Editor-in-Chief of IEEE Trans. on Power Electronics (TPEL).